Using the Physics of the Fast Fading to Improve Performance for Mobile Radio Channels *

Tugay Eyceöz and Alexandra Duel-Hallen
North Carolina State University
Dept. of Electrical & Computer Engineering
Box 7914, Raleigh, NC 27695-7914
teyceoz@eos.ncsu.edu, sasha@eos.ncsu.edu

Hans Hallen
North Carolina State University
Physics Department
Box 8202, Raleigh, NC 27695-8202
Hans_Hallen@ncsu.edu

Abstract

The fading of wireless signals is not a random process, it is deterministic since it is the result of interference between signals following various paths to the receiver. We exploit this deterministic nature of the fading signals and propose a novel approach to communication over the fast fading channels. The key step in this communication system is the prediction of future samples of the fading coefficient from previous observations. This prediction algorithm is closely tied to other important components: feedback from the receiver to the transmitter, transmitter signal optimization, and tracking at the receiver. The objective of this work is to anticipate "deep fades", which severely limit the performance of mobile radio systems. This capability will potentially result in reduced power requirements for wireless channels.

1. The physics of the fast fading

The fading signal results from interference between several scattered signals. Our approach to prediction of future fading is based upon estimates of the important scatterers – their relative phases, direction and amplitudes. To understand the physical origin of how one can predict the fading signal, we must look at the process from two different frames of reference. (1) The first picture is from the point of view of the ground. We will assume all scatterers are stationary and the receiver moves. Then all frequencies are the same (no Doppler shifts in this frame) and an interference pattern results. The receiver passes through this interference pattern. The positions of destructive interference are the deep fades. What we learn from this picture is the expected length scale between the deep fades – on the order of the wavelength, and therefore from the speed of the receiver the time between deep fades. We also can use this picture to estimate the types of scatterers which will produce sufficient intensity to create significant interference, and the spatial distribution of such interference. (2) A different physical picture of the interference pattern derives from the frame of reference of the mobile rather than the ground. In this frame, the signals are Doppler shifted by an amount determined by mobile's speed and the signal angle of incidence relative to its direction (again for stationary scatterers). In particular, the Doppler shift is proportional to the cosine of the angle between the car's direction and the direction of the incident beam of radio waves. The receiver measures sum of these beams, each with different frequency. These frequencies will appear in the complex envelope of the signal and can be measured during the observation interval as described in Section 2. Thus we can effectively measure the number and the direction of the important incident beams (relative to the receiver motion) by measuring the

*This research was supported by NSF grants NCR-9410227 and NCR-9726033.

Doppler shifts. With these data, the position (or time) of future fades can be predicted as we show in [1] and later in this paper. This prediction method is based on the assumption that all scattered amplitudes, phases, and Doppler shifts remain unchanged during the observation and prediction intervals, and that the number of important scatterers is not very large. We will briefly address these considerations below.

In this paper, we focus on the flat fading channel. This channel corresponds to an interference pattern formed due to the intersection of several coherent beams. This pattern will only be of interest to us if the destructive interference is nearly complete – that is if the amplitudes of the beams are nearly the same. If one beam is much weaker, it will create a negligible modulation of the other(s). This gives us our first criterion for choosing relevant beams: the amplitudes must be similar to the strongest received beam. The use of model scatterers is justified by the application of superposition. If we have a complicated scatterer, we can represent it as the sum of simple ones. Therefore, we consider only simple scatterers in our examples. The environment provides many possible scattering sites which could cause additional coherent beams at the receiver. Trees, hillsides, buildings, bridges, guardrails, signs, other vehicles, and the ground can act as scatterers [2, 3, 4, 5]. For an antenna high above the ground, the road and hillsides will provide strong reflections due to their large index of refraction, especially when wet. Trees are rather strong absorbers [3, 4, 6]. They will reflect some, but the intensity will be much lower and the distribution of scattering distances will probably destroy the coherence of the beam. We will neglect tree and forest scattering, except when they block the primary beam. The size of the scatterer becomes an issue for signal prediction. We consider as model systems a large reflector (road, hillside), a very small reflector (sign, guardrail), and intermediate sized flat and curved reflectors (cars, etc). Each can be understood qualitatively. We are interested in the following quantities: (1) the interference pattern, (2) signal strength, (3) path length difference, and (4) Doppler shifts.

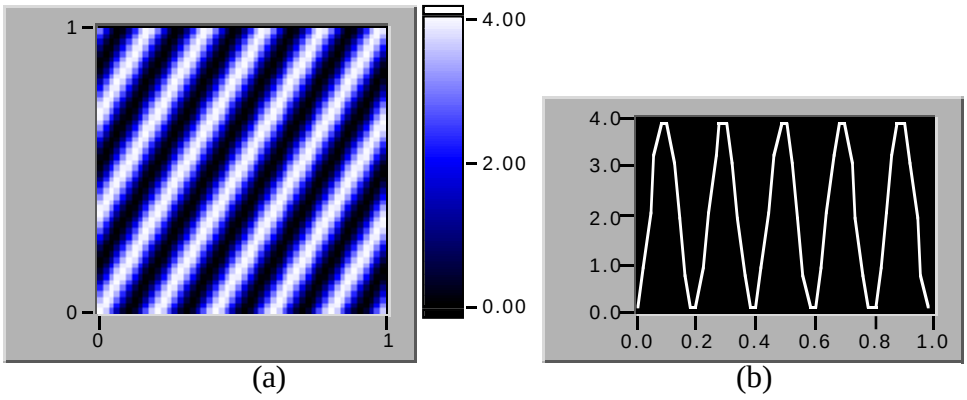

Figure 1. (a) The interference pattern for two plane wave sources one incident from the left and the other from the lower right 60° below horizontal. The frequency is 1 GHz and the image 1 m on a side. (b) A horizontal cut through the image half way up the image in (a).

To start off with a simple example, consider two plane waves of equal intensity incident at 120 degrees from each other. This approximates the signal in a region far from the source and a scatterered signal for a single scatterer positioned to give the 120° relative incidence. Figure 1 shows the interference pattern and a line through it. The waves have been interfered and squared. In particular the electric field E is given by the sum of two waves

$$E = Acos\left[\frac{2\pi}{\lambda}(\alpha x + \beta y) + 2\pi f t\right] + A'cos\left[\frac{2\pi}{\lambda}(\alpha' x + \beta' y) + \phi' + 2\pi f t\right] \quad (1)$$

of frequency f, wavelength λ, relative phase ϕ', and direction cosines $\alpha = cos$(angle between propagation direction and x) and $\beta = cos$(angle between direction and y). The primes indicate scattered wave parameters. This can be simplified to separate the time dependence and squared to give

$$|E|^2 = \xi_c^2 cos^2(2\pi ft) + \xi_s^2 sin^2(2\pi ft) + \xi_c \xi_s sin(4\pi ft) \tag{2}$$

where

$$\begin{aligned} \xi_c &= A cos\left[\frac{2\pi}{\lambda}(\alpha x + \beta y)\right] + A' cos\left[\frac{2\pi}{\lambda}(\alpha' x + \beta' y) + \phi'\right] \\ \xi_s &= A sin\left[\frac{2\pi}{\lambda}(\alpha x + \beta y)\right] + A' sin\left[\frac{2\pi}{\lambda}(\alpha' x + \beta' y) + \phi'\right] \end{aligned}$$

Time averaging removes the final term in Equation (2), and sets the sin^2 and cos^2 to 1/2. Thus the pattern shown in Figure 1 is simply $\xi_c^2 + \xi_s^2$, since the measured signal power will be proportional to $|E|^2$. For a car moving horizontally through the pattern, the line in Figure 1(b) indicates the relative power of an unmodulated received signal. In the more general case of unequal amplitudes, the pattern will not go all the way to zero, and the power variation will be decreased. It is also interesting to note the relative angle dependence. If both waves come from the same direction, the pattern is constant everywhere. If they approach from opposite directions, a standing wave pattern with minima every $\lambda/2$ is formed. Angles in between show a wave pattern with a longer spatial period – approaching infinity as their directions coincide.

More generally one can write the interference pattern generated by N scatterers based on the direction after scattering (α, β, γ) and relative phase ϕ with amplitude A:

$$|E|^2 = \sum_{i=1}^{N} \sum_{j=1}^{N} 0.5 A_i A_j cos(\psi_j - \psi_i) \tag{3}$$

with phase factors $\psi_j = \frac{2\pi}{\lambda}(\alpha_j x + \beta_j y + \gamma_j z) + \phi_j$.

Using this formulation, we investigate the spatial pattern of the interference. The reflecting objects (scatterers) are classified according to size, and three cases are studied. First, a small scatterer defined as an object close to or smaller than one wavelength λ in size is investigated. The wavelength for 1 GHz microwaves is 0.3 m, so roadsigns, mileposts, a coke can, and, in one dimension only: guardrails, telephone poles/lines, people, and distant bridges are considered small. Second, a large scatterer is investigated. It is defined as an object large compared to the distance the mobile moves in a reasonable time. This then includes hillsides, large buildings and the road. A medium-sized scatterer falls between the other two cases. This class of objects includes cars, very large roadsigns and small buildings. As a result of this study, the relative importance of possible scatterers is determined, and the interference pattern is characterized for various scenarios.

Briefly, we have determined that single small (wavelength-sized or smaller) objects will usually not be important in the interference pattern due to the spreading of the energy over a large area by diffraction [7] which decreases the irradiance. Large objects can be modeled in reflection as a virtual source behind the reflector. For large, flat objects far from the transmitter the effective source will lie far behind the object. Thus, the variation in the Doppler shift with motion will be minimal. Curved objects are modeled as spherical mirrors, so the effective source is closer and Doppler variations can be faster. This is important within several meters of the object. The variation of amplitude with position for large objects is slow. Medium-sized objects can have a rapid variation of amplitude with position. If they are flat, this will spread slowly (by diffraction) with distance. If they are curved, geometry will spread the pattern and thus slow the rate of variation, and reduce the irradiance with distance. Shadowing effects are also shown to produce relatively rapid changes of amplitude with position only for particular mobile paths.

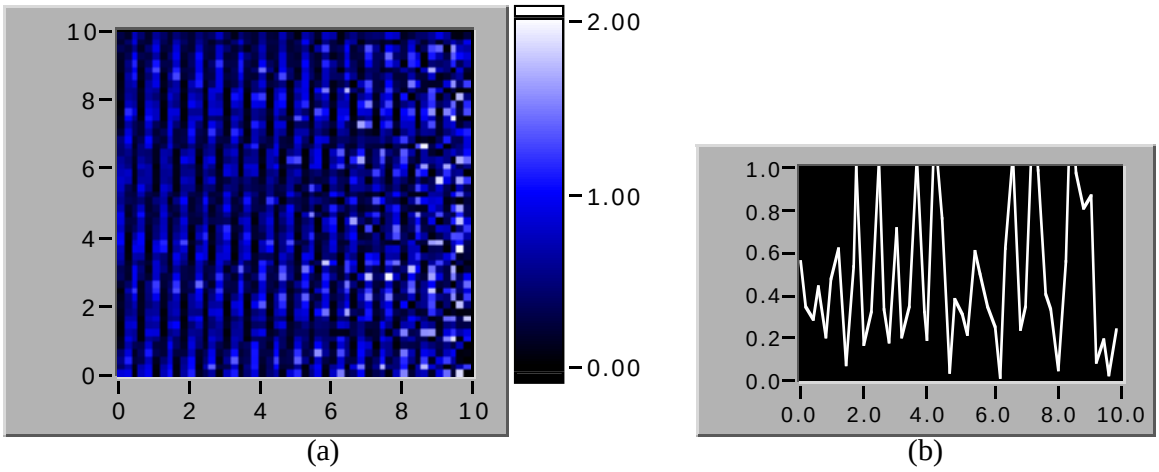

Figure 2. One large and five medium-sized reflecting objects create an interference pattern with the source. (a) The interference pattern in a 10 m square region. (b) A horizontal line cut through the image reveals the pattern. Note the quasi-periodic deep fades. The horizontal axis in meters can be converted to time by dividing by the mobile's velocity

We can discuss some of the important scatterers in several environments. The rural highway will have large Doppler shifts due to the large velocities. Most objects of importance are far from the mobile with the exception of other cars. These cars (medium-sized objects) usually have small relative velocities to the mobile therefore the rapid variation with position of both the amplitude and Doppler shift are much less important. A parked car near the road is rare, but would pose a much more significant challenge. Shadowing is expected to be slow, so our method for channel prediction should work well. Suburban neighborhoods would provide a significant number of parked cars and houses – medium-sized scatterers at relatively close range – which are expected to cause the most serious constraints. The slow vehicle speed helps. Urban areas are filled with medium to large buildings and cars so are expected to have a larger number of significant scatterers. The buildings may also cause shadowing at close distances, depending upon base station positioning, producing rapid variations in space. These are reasonable if the speed is slow, but problems may arise from shadowing by buildings and underpasses on urban highways, depending upon the specific geometry of the source and strong scatterers. Base station siting may be critical for the performance of our method.

Based on these observations and using typical numbers, it appears that most situations (but not all) would be adequately handled by a system which could respond to changes in Doppler frequency and amplitude on the 0.1 second time scale. Therefore, the fading prediction and transmitter optimization will have to satisfy this requirement. When the Doppler frequency and amplitudes change significantly faster, or the number of significant scatterers is very large, than accuracy of the prediction will be reduced. In addition, when vehicle speeds are low, it would be difficult to resolve Doppler shifts. However, as explained below, the proposed method is not a stand-alone technique, but is supposed to enhance and supplement the performance of current adaptive tracking techniques. The study summarized above suggests that the proposed method should be successful in the majority of practical scenarios.

We end this section with an example of one large and five medium-sized reflecting objects creating an interference pattern with the source as seen in Figure 2. The source is 100 m to the left of the image, half way up. The large object does not run vertically, so its effective source is 100 m to the right of the image bottom – think of

it as a hill. Its amplitude reflection coefficient is about 2/3. The five medium-sized scatterers are evenly spaced parallel to the right edge, with effective sources 1 m outside the image. Think of them as five spherical cars parked perpendicular to the road. We see that the interference pattern is complex on the left side, and that the irradiance has narrow, deep minima, or deep fades, which are less than 1/40 the average power. This curve is not that different from what is observed in the field, showing that several scatterers are sufficient to produce such an interference pattern as has also been noted in [8].

2. Prediction of the fading channel

Consider a low-pass complex model of the received signal:

$$r(t) = c(t)s(t) + n(t),$$

where $c(t)$ is the flat fading coefficient (multiplicative), $s(t)$ is the transmitted signal, and $n(t)$ is additive white Gaussian noise (AWGN).

Let the transmitted signal be $s(t) = \sum_k b_k g(t - kT)$, where b_k is the data sequence, $g(t)$ is the transmitter pulse shape, and T is the symbol delay. At the output of the matched filter and sampler, the discrete-time system model is given by

$$r_k = c_k b_k + z_k, \tag{4}$$

where c_k is the fading signal $c(t)$ sampled at the symbol rate, and z_k is the discrete AWGN process. Usually, $c(t)$ and c_k can be modeled as a correlated complex Gaussian random processes with Rayleigh distributed amplitudes and uniform phases [9, 10]. Several adaptive channel estimation methods have been developed by using this statistical description to estimate rapidly varying fading coefficients (e.g. [11, 12, 13, 14]). However, the performance of these methods degrades when the fading rate increases due to large estimation error. In addition, these algorithms do not address the most serious limiting factor in communication over fading channels. The greatest bit error rate (BER) loss and the associated high power requirements result from "deep fades" in the fading signal. Therefore, it is desirable to predict deep fades, and, in general, fading variations and compensate for the expected power loss at the transmitter. Therefore, we address the *deterministic* prediction of the variations in c_k. By prediction we imply estimating an entire future block of coefficients c_k based on the observation of the received signal during an earlier time interval.

The derivation of our prediction method is based on a physical description of the fading signal presented in Section 1 (see also [2, 10]). In this section, we concentrate on the mathematical description of the interference pattern from the point of view of the mobile. The fading coefficient at the receiver is given by a sum of N Doppler shifted signals

$$c(t) = \sum_{n=1}^{N} A_n e^{j2\pi f_n t + \phi_n} \tag{5}$$

where (for the n^{th} scatterer) A_n is the amplitude, f_n is the Doppler frequency, and ϕ_n is the phase. The Doppler frequency is given by

$$f_n = f_c(\frac{v}{c})cos\alpha_n \tag{6}$$

where f_c is the carrier frequency, v is the speed of mobile, c is the speed of light, and α_n is the incident angle relative to the mobile's direction. Due to multiple scatterers, the fading signal varies rapidly for large vehicle speeds and undergoes "deep fades" [2, 9].

We predict the fading signal c_k (4) by decomposing it in terms of the N scattered components. If the parameters A_n, f_n, and ϕ_n in (5) for each of the scatterers were known and remained constant, the signal could be predicted indefinitely. In practice, they vary slowly and are not known a priori (see Section 1). We assume that the

propagation characteristics will not change significantly during any given block. Therefore, we model these parameters are approximately constant or change slowly varying for the duration of the data block.

To predict the fading signals (4-5), we employ spectral estimation followed by linear prediction and interpolation [1]. Estimation of the power spectral density of discretely sampled deterministic and stochastic processes is usually based on procedures employing the Discrete Fourier Transform (DFT) [15]. Although this technique for spectral estimation is computationally efficient, there are some performance limitations of this approach. The most important limitation is that of frequency resolution. The frequency resolution ($\Delta f = f_s/N$) of the N-point DFT algorithm, where f_s is the sampling frequency, limits the accuracy of estimated parameters. These performance limitations cause problems especially when analyzing short data records.

Many alternative Spectral Estimation Techniques have been proposed within the last three decades in an attempt to alleviate the inherent limitations of the DFT technique [15, 16, 17]. We explore the Maximum Entropy Method (MEM) for the prediction of the fast fading signal. This method is also known as the All-poles Model or the Autoregressive (AR) Model and is widely used for spectral estimation. The reason why we chose this technique is that the MEM has very nice advantage of fitting sharp spectral features as we have in our fading channel due to scatterers (5). Furthermore, MEM is closely tied to Linear Prediction (LP) which we use to predict future channel coefficients. Using MEM, the frequency response of the channel is modeled as:

$$H(z) = \frac{1}{1 - \sum_{j=1}^{p} d_j z^j}. \tag{7}$$

This model is obtained based on a block of samples of the fading process. Note that the samples have to be taken at least at the Nyquist rate which is twice the maximum Doppler frequency, f_d. Moreover, the accuracy of the model depends on the number of samples in the given block. The d_j coefficients are calculated from the poles of the power spectral density.

The d_j coefficients in (7) are also the linear prediction coefficients. The estimates of the future samples of the fading channel can be determined as:

$$\hat{c}_n = \sum_{j=1}^{p} d_j c_{n-j}, \tag{8}$$

Thus, $\hat{c}_n$ is a linear combination of the values of c_n over the interval $[n-p, n-1]$. Since actual channel coefficients are not available beyond the observation interval, earlier sampling estimates, $\hat{c}_{n-j}$, can be used instead of the actual values c_{n-j} in (8) to form future estimates $\hat{c}_n$, or the samples can be updated adaptively as discussed in Section 3.

Note that the channel sampling rate utilized for LP is much lower than the symbol rate, $1/T$. Therefore, to predict the fading coefficients, c_k (4), associated with transmitted symbols, interpolation is employed as discussed in the next section.

3. Simulation Results and Discussion

Several numerical results presented below illustrate performance characteristics of the proposed technique. In the examples, we assume that the maximum Doppler frequency is 100 Hz, and the data rate is 24 Ksps. We sample the channel at the rate of 240 Hz. Thus, there are 100 data points between adjacent sampling points. To determine initial observations of the fading coefficients, c_k, at the sampling points, one can send training symbols b_k at the channel sampling rate of 240 Hz (see (4)). This overhead affects the throughput only by 1%.

In order to give a better insight into the performance of this technique, we will first demonstrate the case of three scatterers ($N = 3$ in (5)). With the sampling frequency, $f_s = 240$ Hz, the three Doppler frequencies correspond to $100, 50,$ and 30 Hz. The plot of the envelope due to these scatterers is drawn in Figure 3. The channel is observed for the first 25 samples. Then, by employing MEM and linear prediction, the future values of the channel envelope

are estimated and plotted using dotted lines for the last 25 samples in the figure. The estimates agree with actual values and we can detect when the channel is going to enter deep fades in the future. When the same experiment is repeated in the presence of additive white Gaussian noise, the predicted values still follow very closely the actual channel envelope [1].

We also performed simulations for a greater number of scatterers. In Figures 4 and 5, the original Jakes channel model with nine oscillators (scatterers) is examined [10]. In Figure 4, the pole-zero plot of the frequency response of the Jakes channel model with a maximum Doppler frequency, $f_d = 100$ Hz, is illustrated. As the number of oscillators increases, we need a greater number of poles. Note that the poles corresponding to the oscillators are very close to the unit circle. The channel is observed for the first 150 samples. We plotted the predicted channel envelope in dotted lines and the actual channel envelope in solid lines after the observation interval in Figure 5. It can be seen that the predicted values still follow very closely the actual channel envelope. However, later in the prediction, the accuracy decreases because of the cumulative effect of the LP error. This error is due to the fact that earlier estimates rather than actual fading values are used in predicting future samples. This problem can be solved by combining adaptive tracking at the receiver with prediction as described later in this section.

Since the sampling rate for the fading channel is much lower than the data rate, we perform interpolation between predicted channel coefficients to get better resolution. In this interpolation process, four consecutively predicted channel coefficients are interpolated by a Raised Cosine (RC) filter to generate estimates of the fading coefficients, $\hat{c}_k$, between two adjacent predicted samples at the data rate [18]. The interpolation result and the actual channel coefficients are shown in Figure 6. The solid line represents the actual channel coefficients, c_k, at the data rate. Two points, represented by $*$, are the estimated channel parameters. By using these points (as well as one previous and one next estimate), we perform the interpolation at the data rate. These interpolated estimates, $\hat{c}_k$ are shown with dashed line in the figure. We prefer interpolation to oversampling of the fading channel to obtain the fading coefficients at the data rate. If oversampling is employed, MEM will require a larger number of poles and consequently the complexity will increase.

The proposed prediction method can be combined with tracking and transmitter signal power adjustment. The following protocol is investigated to accomplish reliable communication. The channel samples taken during the observation interval are sent to the transmitter, which applies linear prediction to compute the coefficients d_k and interpolates to produce predicted fading values at the data rate. Note that this feedback is not going to introduce significant delay since the sampling rate is much lower than the data rate. Then, the transmitter sends the data bits, b_k, by multiplying them with the inverse of the $\hat{c}_k$ values. While this is not the optimal method for transmission over the time varying channel, it still achieves significant gains relative to the case when power compensation is not employed at the transmitter. At the output of the matched filter and sampler, the new modified discrete-time received signal is given by

$$y_k = \frac{c_k}{\hat{c}_k} b_k + z_k. \tag{9}$$

where z_k is discrete-time AWGN.

Define $a_k \stackrel{\triangle}{=} c_k/\hat{c}_k$. As the prediction gets better, the value of a_k goes to 1. When $a_k = 1$, i.e., perfect estimation, our fast fading channel becomes the AWGN channel. In our initial simulations, we assumed coherent detection and used Binary Phase Shift Keying (BPSK) modulation scheme. Therefore, when $a_k = 1$, for the AWGN channel, the average probability of bit error is given by [9]

$$P_e = Q(\sqrt{2\gamma_b}) \tag{10}$$

where γ_b is the signal-to-noise (SNR) and $Q(x)$ is defined as $Q(x) = \frac{1}{\sqrt{2\pi}} \int_x^\infty e^{-t^2/2} dt$. Since this performance is achieved with perfect prediction, this curve forms a lower bound for our system. Now, let us assume there is no correction at the transmitter. Then, the received signal is given by equation (4). Since c_k is approximately

Rayleigh distributed, the average probability of bit error for the Rayleigh fading channel is found as [9]

$$P_e = \frac{1}{2}\left(1 - \sqrt{\frac{\gamma_b}{1+\gamma_b}}\right) \tag{11}$$

Obviously, if the lower bound can be approximated, very significant SNR gain would result. Our results show that the average probability of bit error with the compensation at the transmitter lies between the upper and lower bounds. To approach the lower bound, we employ the Least Mean Squares (LMS) adaptive algorithm to track the variations in a_k. Given the received signal (9), the LMS algorithm is performed at the data rate as

$$\tilde{a}_{k+1} = \tilde{a}_k + \mu b_k (y_k - \tilde{y}_k)^* \tag{12}$$

where μ is the step size, $\tilde{y}_k = \tilde{a}_k b_k$. This tracking is employed to perform coherent detection at the receiver, as well as to update the estimate of the fading at the sampling rate. The new fading sample is computed as $\tilde{c}_k = \tilde{a}_k \hat{c}_k$ and send back to the transmitter at the sampling rate. The transmitter uses this updated estimates in (8) to predict future fading values, rather than relying on previous estimates. This adaptive algorithm enables us to reduce the prediction error described earlier and to approximate the performance of the AWGN channel.

4. Conclusions

The flat fading channel is characterized in terms of the characteristics of important scatterers. This analysis demonstrates the feasibility of the fading prediction technique described in this paper. Using the proposed prediction method, it would be possible to determine the channel coefficients prior to transmission. In particular, the timing of future "deep fades" would be revealed and the variations in received signal power could be compensated.

The capability to predict fading coefficients will reduce the power requirements of wireless communications systems and increase the system performance. For example, it would be possible to avoid transmission during deep fades or to utilize diversity techniques (e.g., use space diversity or hop to another non-fading frequency during the deep fade) [2, 9]. In addition, more efficient modulation and coding techniques are envisioned. Note that the proposed method is not meant to replace adaptive channel estimation required for coherent detection. Instead, prediction will result in more reliable tracking of the received signal.

Several important questions related to the proposed method are addressed in our current work. The prediction algorithms described in Section 3 are applied to BPSK systems and require the knowledge of transmitted data at the sampling instances during the observation interval. However, the realistic channel has phase ambiguity and requires differential encoding. Thus, we are studying the extension of the proposed method to differentially encoded signals. Applications of the prediction algorithms to multipath fading channel is another important area of investigation. Finally, we are continuing realistic channel modeling necessary to verify feasibility of the proposed method. For various scenarios studied, we determine the character of significant scatterers, and evaluate feasibility of our prediction methods. Adaptive tracking of the prediction coefficients is also addressed in this work.

References

[1] T. Eyceöz, A. Duel-Hallen, and H. Hallen "Prediction of Fast Fading Parameters by Resolving the Interference Pattern", *Proceedings of ASILOMAR Conference on Signal and Systems*, Nov. 2-5, 1997.

[2] T. S. Rappaport, *Wireless Communications*, Prentice Hall, NJ, 1996.

[3] A. Seville, U. Yilmaz, P. G. V. Charriere, N. Powel, and K. H. Craig, "Building Scatter and Vegetation Attenuation Measurements at 38 GHz", *Proceedings of the 9th International Conference on Antennas and Propagation*, Eindhoven, the Netherlands, 46–50, 1995

[4] T. J. Schmugge and T. J. Jackson, "A Dielectric Model of the Vegetative Effects on the Microwave Emission from Soils", *IEEE Transactions on Geoscience and Remote Sensing*, 30(4): 757–760, 1992

[5] M. S. Ding and M. O. Al-Nuaimi, "Prediction of Scatter Coefficient of Buildings at Microwave Frequencies in Site Shielding", *Proceedings of the 9th International Conference on Antennas and Propagation*, Eindhoven, the Netherlands, 42–45, 1995

[6] I. J. Dilworth and B . L'Ebraly, "Propagation Effects due to Foliage and Building Scatter at Millimeter Wavelengths", *Proceedings of the 9th International Conference on Antennas and Propagation*, Eindhoven, the Netherlands, 51–53, 1995

[7] O. S. Heavens and R. W. Ditchburn, *Insight into Optics*, Wiley, Chichester, 1991

[8] P. A. Mathews and B. Mohebbi, "Direction of Arrival and Building Scatter at UHF", *Proceedings of 7th International Conference on Antennas and Propagation*, York, U.K., 147–150, 1991

[9] J. G. Proakis, *Digital Communications*, McGraw-Hill, New York, 1995.

[10] W. C. Jakes, *Microwave Mobile Communications*, John Wiley and Sons, New York, 1974.

[11] J. Lin, J. G. Proakis, F. Ling, and H. Lev-Ari, "Optimal Tracking of Time-Varying Channels: A Frequency Domain Approach for Known and New Algorithms", *IEEE Transactions on Selected Areas in Communications*, 13(1):141–154, Jan. 1995.

[12] R. Haeb and H. Mayr, "A Systematic Approach to Carrier Recovery and Detection of Digitally Phase Modulated Signals on Fading Channels", *IEEE Transactions on Communications*, 37(7):748–754, July 1989

[13] Z. Zvonar and M. Stanjovic, "Performance of Antenna Diversity Multiuser Receivers in CDMA Channels with Imperfect Channel Estimation", *Wireless Personal Communications Journal, Kluwer*, 91–110, July 1996

[14] H. Y. Wu and A. Duel-Hallen, "Performance Comparison of Multiuser Detectors with Channel Estimation for Flat Raleigh Fading CDMA Channels", *Special Issue on Interference in Mobile Wireless Systems, Wireless Personal Communications Journal, Kluwer*, in press

[15] J. G. Proakis, D. G. Manolakis, *Digital Signal Processing*, Prentice Hall, NJ, 1996.

[16] M. H. Hayes, *Statistical DSP and Modeling*, John Wiley and Sons, 1996.

[17] S. M. Kay and S. L. Marple "Spectrum Analysis–A Modern Perspective", *Proceedings of the IEEE*, 69(11), 1380–1419, Nov. 1981

[18] T. Eyceöz and A. Duel-Hallen, "Reduced Complexity Diversity Combining and Adaptive Equalization Using Interpolated Channel Estimates with Applications to Cellular Mobile Radio Channels", *Proceedings of ICUPC*, 51–55 Sep. 30-Oct. 2, 1996.

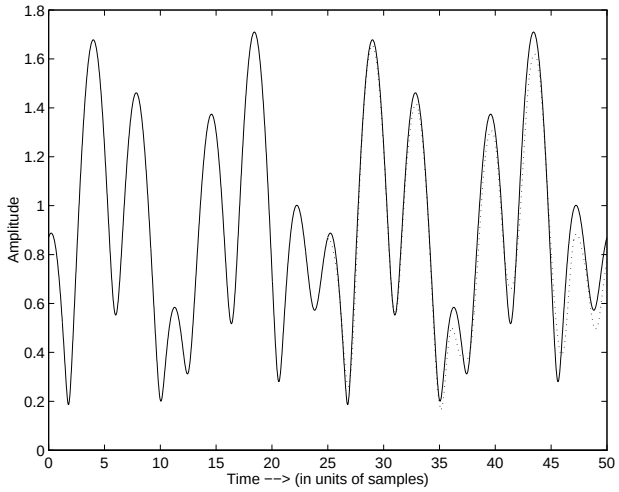

Figure 3. Actual (—) and estimated (...) fading channel envelopes for 3 scatterers, $f_d = 100$ Hz

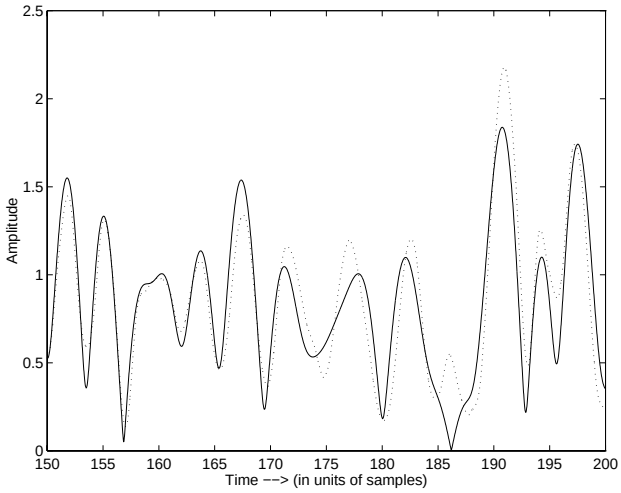

Figure 5. Actual (—) and estimated (...) fading channel envelopes for the Jakes channel model, $f_d = 100$ Hz

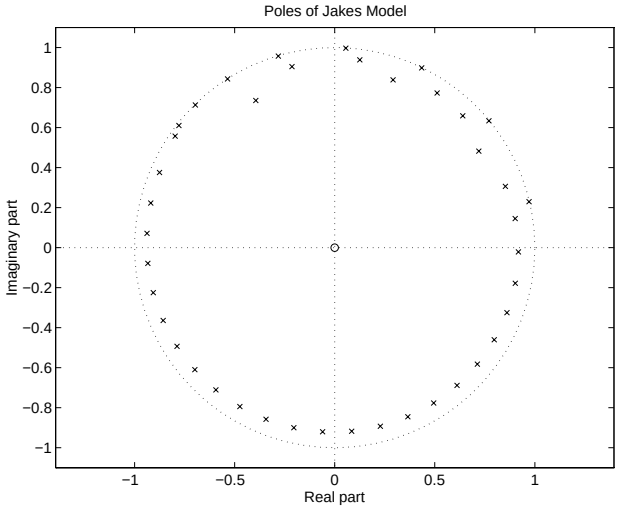

Figure 4. Pole-zero locations of the frequency response of the Jakes channel model, $f_d = 100$ Hz

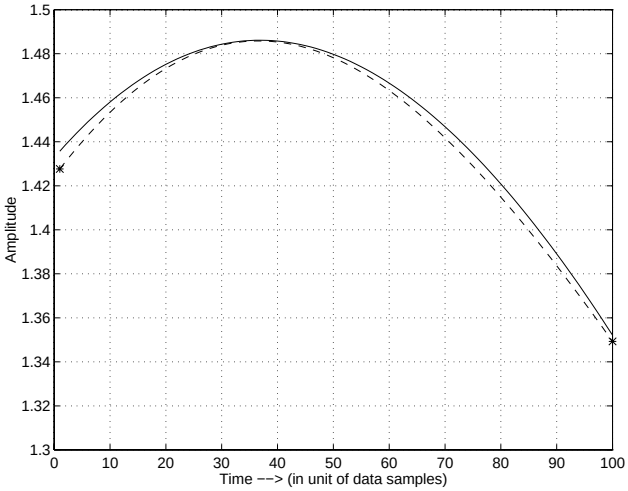

Figure 6. (—): actual channel coefficients, c_k; $(- - -)$: interpolated channel estimates, $\hat{c}_k$